frontiers | Frontiers in Earth Science

TYPE Original Research
PUBLISHED 31 August 2022
DOI 10.3389/feart.2022.987294

OPEN ACCESS

EDITED BY
Yusen He,
Grinnell College, United States

REVIEWED BY
Decheng Zhang,
Hebei University of Technology, China
Yamg Luo,
Xi'an University of Architecture and Technology, China
Hao-sen Guo,
East China Jiaotong University, China

*CORRESPONDENCE
Xiulei Li,
hellolixiulei@163.com
Chao Yang,
yangchao0615@ctgu.edu.cn

SPECIALTY SECTION
This article was submitted to Geohazards and Georisks, a section of the journal Frontiers in Earth Science

RECEIVED 06 July 2022
ACCEPTED 25 July 2022
PUBLISHED 31 August 2022

CITATION
Li X, Li X and Yang C (2022), A comparison study of face stability between the entering and exiting a shallow-buried tunnel with a front slope.
Front. Earth Sci. 10:987294.
doi: 10.3389/feart.2022.987294

A comparison study of face stability between the entering and exiting a shallow-buried tunnel with a front slope

Xinzhe Li[1], Xiulei Li[2]* and Chao Yang[1]*

[1]Key Laboratory of Geological Hazards on Three Gorges Reservoir Area, Ministry of Education, China Three Gorges University, Yichang, China, [2]College of Traffic and Transportation, Chongqing Jiaotong University, Chongqing, China

Worldwide, it is a great challenge to tunnel in portal section, where excessive deformation, cracking, or even collapse often occurs during the construction process. This paper presents a comparison study of face stability between entering and exiting a shallow-buried tunnel with a front slope. Firstly, the theoretical solutions of support pressure σ_T and safety coefficient *FS* of the excavation face considering surface slope are derived by upper-bound limit analysis method. Secondly, for different slope angles, buried depth and surrounding rocks of the exit and entrance sections, the σ_T and *FS* are obtained. The results show that when the burial depth of the tunnel crown *h* remain constant, the σ_T increased first and then decreased while the *FS* increased gradually, and both become steady when the slope angle α arrive at a certain value. In addition, the thicker the *h* is, the smaller the certain value α is. When the *h* and α remain constant, the loose area in front of the excavate face will decreased apparently with the increase of the internal friction angle φ, thus the σ_T will decrease and *FS* will increase. Moreover, the σ_T decreased linearly with the increase of cohesion *c* and unit weigh γ of surrounding rock, while the *FS* is the opposite. Compared with the entrance section, the construction risk at the exit section is greater.

KEYWORDS

shallow-buried tunnel, face stability, upper-bound limit analysis, tunnel entrance, tunnel exit

Abbreviations: *FS*, safety coefficient; *R*, polar radius of the logarithmic spiral curve (m); R_0, length of *OA* (m); R_{OD}, length of *OD* (m); R_{OF}, length of *OF* (m); L_{OB}, length of *OB* (m); L_{OC}, length of *OC* (m); L_{BC}, length of *BC* (m); L_{CD}, length of *CD* (m); L_{BF}, length of *BF* (m); θ, polar angle of the logarithmic spiral curve (°); θ_0, included angle between *OA* and $-y$ axial (°); θ_b, included angle between *OB* and $-y$ axial (°); θ_c, included angle between *OC* and $-y$ axial (°); θ_d, included angle between *OD* and $-y$ axial (°); θ_f, included angle between *OF* and $-y$ axial (°); *h*, burial depth of the tunnel crown (m); *d*, tunnel height (m); α, included angle between ground surface and the horizontal plane (°), it is positive at the entrance and negative at the exit; γ, unit weight (kN/m^3); *c*, cohesion (kPa); φ, internal friction angle (°); σ_T, support pressure distributed on the excavation surface (kPa); σ_0, additional pressure acting on the surface (kPa); ω, rotational angular velocity.

1 Introduction

The tunnel portal section is often affected by unfavorable terrain and geological conditions such as shallow burial depth, unsymmetrical loading and broken surrounding rocks, resulting in various damages such as excessive deformation, cracking, or even collapse during the construction process (Ye et al., 2012; Liu et al., 2015). Currently, there have been a large number of studies and reports on tunnel portal section, covering various aspects such as pre-reinforcement technology (Coulter and Martin, 2006; Xiao et al., 2016; Yang et al., 2019), slope and face stability (Adam et al., 2014; Lei et al., 2015; Yuan et al., 2020; Zhou et al., 2021; Li et al., 2022), excavation methods and support (Miura, 2003; Yang et al., 2021), damage and treatment (Kontogianni et al., 2004; Yang et al., 2019; Cui et al., 2021), and others (He and Kusiak, 2017; Li et al., 2021a; Li et al., 2021b). However, the existing

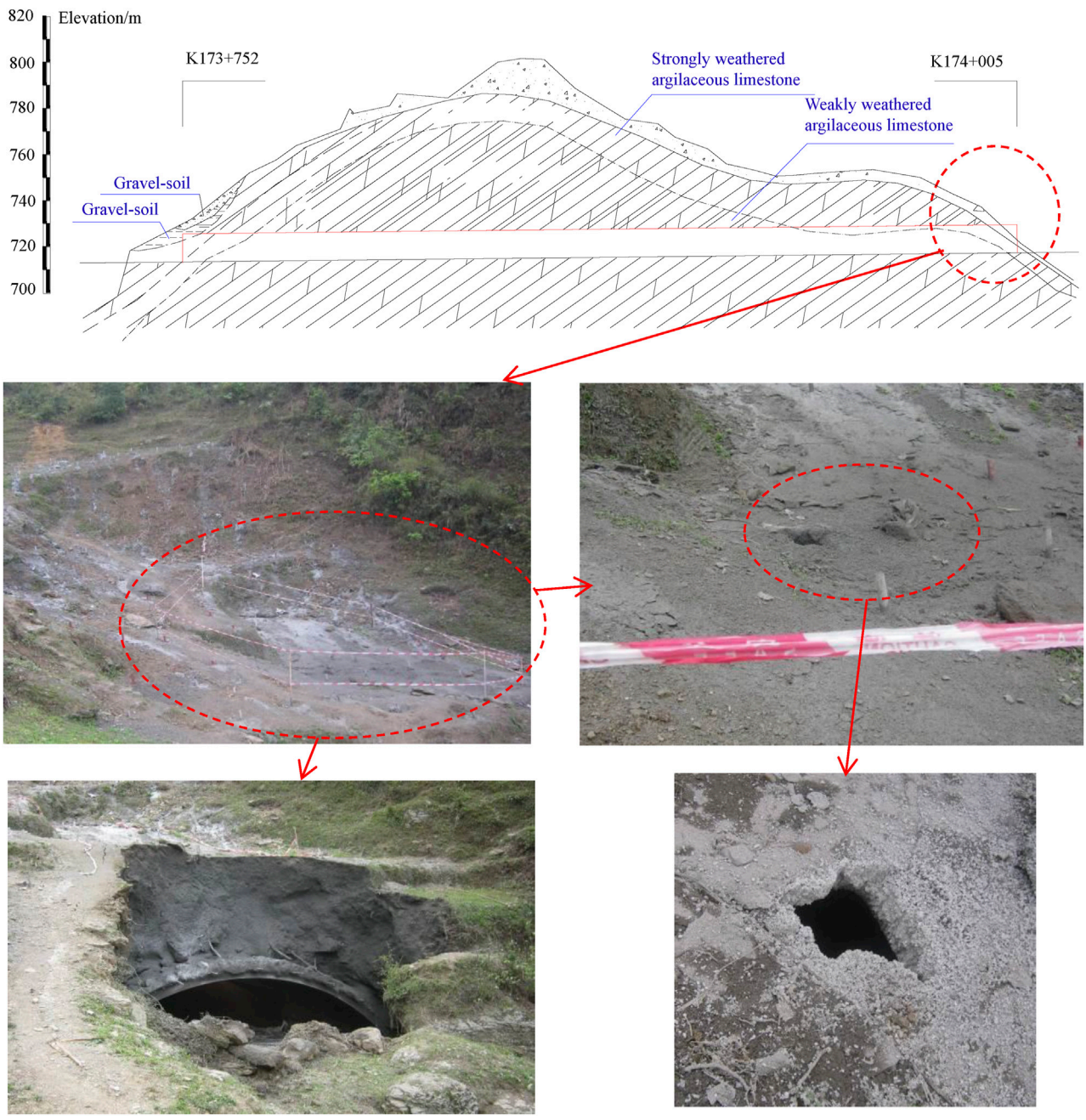

FIGURE 1
Collapse during exiting the Pingzhai Tunnel (western China).

FIGURE 2
A typical front slope tunnel portal.

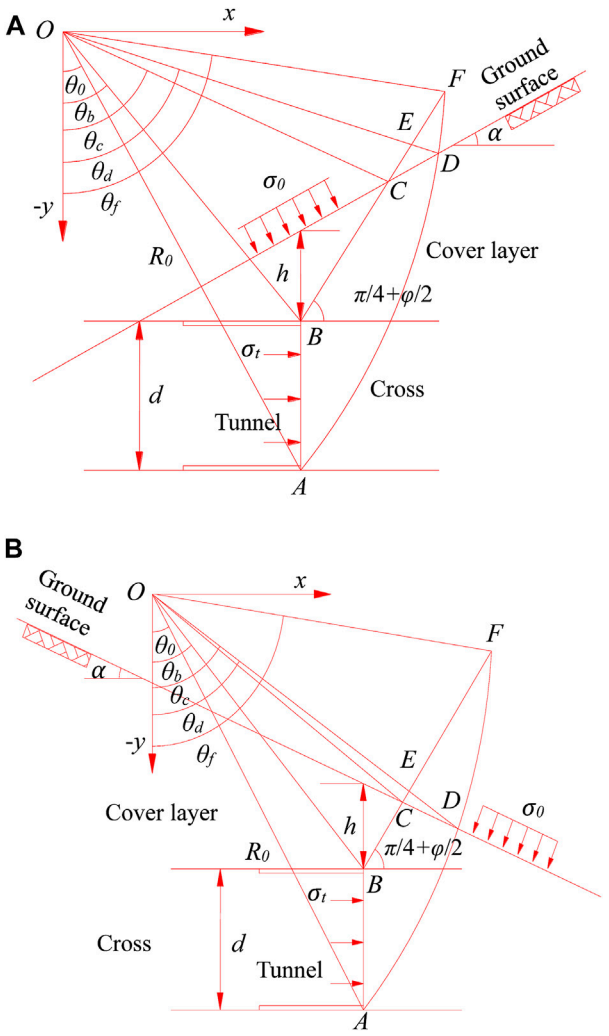

FIGURE 3
The failure model of tunnel face at portal section: **(A)** entrance section; **(B)** exit section.

literatures has mainly focus on the condition of entering the tunnel, while relatively few studies have been carried out on the exit section. Actually, the occurrence of all kinds of damage in the tunnel exit section is not uncommon, such as the Pingzhai Tunnel of Xiamen—Chengdu Highway, due to shallow burial and low quality of surrounding rock, collapse occurred during exiting process. Firstly, a circular collapse about 50 cm appeared on the surface (Figure 1), and the collapse gradually increased with the further excavation. The distortion of primary support, breakage of pipe roof and collapse of slope in the tunnel exit section of Wafanggou Tunnel of Shangzhou - Manchuanguan Highway (Li, 2009). Li and Yang (2016) used a 3D numerical model to simulate the excavation of Pingzhai Tunnel portal, the result showed that the stress and deformation of surrounding rock are different between entering and exiting the portal using the same excavation method.

Limit analysis method or limit equilibrium method is often used in the theoretical analysis of tunnel excavation face stability. In 1987, Broms and Bennermark, (1967) firstly put forward the concept of stability factor N of tunnel face in undrained clay stratum and suggested that $n < 6$ should be taken as the condition for the excavation face to remain stable. In the following decades, this method has been widely used and improved. For instance, Anagnostou and Perazzelli (2013) and Wu et al. (2015) proposed formulas for calculating the limit support pressure considering the arching effect in soil, respectively. Liang et al. (2017) changed the failure area of the square wedge body in front of excavation face into the spiral body, and deduced the calculation model considering excavation footage. Leca and Dormieux (1990) proposed a failure criterion for the tunnel face in the general case of a cohesive and friction soil, and provided charts to allow a bracketed estimate of the required retaining pressure. Based on the Leca's model, Mollon et al. (2009) and Zhang et al. (2015) proposed the failure modes composing of multiple rigid truncated cones, and obtained the upper-bound solution for the face stability through optimization, respectively. Zhao et al. (2017) obtained the optimal upper limit solution for support pressure by using the sequential quadratic programming method. The above mentioned literatures are mainly carried out under the condition that the surface is horizontal. However, the tunnel portal section is usually shallow buried, hence the effect of surface slope should not be ignored.

In this paper, the tunnel portal with a front slope, which is one of the most typical portal types, is taken to investigate the difference between entering and exiting the tunnel. As shown in Figure 2, the covering depth of this tunnel on the left and right sides is almost the same, and therefore no obviously unsymmetrical loading is formed. However, the covering depth

gradually increases along the tunnel axis to form a front slope with a dip direction parallel to the tunnel axis. The construction of this tunnel portal section, i.e., excavation at the foot of the front slope, will easily lead to the instability of slope and surrounding rock. Firstly, the theoretical solutions of support pressure σ_T and safety coefficient FS of the excavation face considering surface slope are derived by upper-bound limit analysis method. Then the face stability under entering and exiting conditions is systematically compared through calculation the σ_T and FS of different burial depth, surrounding rock parameters and the slope angles. The conclusion can serve as references for the excavation and support of similar engineering.

2 Limit analysis of the tunnel face stability

2.1 Failure mode

Since such tunnel portal is symmetrically distributed along the center line, a two-dimensional model can be used for simplified analysis. The assumed failure mode of tunnel face is shown in Figure 3, AB is the excavation face; BF is the sliding surface on the top of the vault; AF is the sliding surface on the lower part of the bottom vault. According to the research results of Chambon and Corté (1994) and Takano et al. (2010), it is assumed that the loose area in front of the face is in the shape of a logarithmic spiral, i.e. AF in Figure 3 is a logarithmic spiral curve (O is the center point), and the equation is

$$R = R_0 \exp\left[(\theta - \theta_0)\tan\varphi\right] \tag{1}$$

The included angle between AF and the horizontal plane at the tunnel bottom surface, the included angle between BF and the horizontal plane, and the included angle between OA and the–y axial are all $(\pi/4+\varphi/2)$ (Chambon and Corté, 1994; Takano et al., 2010).

2.2. Geometry parameter

As shown in Figure 3, the equations for BF and the ground surface CD are

$$y_{BF} = \tan(\pi/4 + \varphi/2)\cdot x + d - R_0\left[\cos\theta_0 + \tan(\pi/4 + \varphi/2)\sin\theta_0\right] \tag{2}$$

$$y_{CD} = \tan\alpha\cdot x + d + h - R_0(\cos\theta_0 + \tan\alpha\sin\theta_0) \tag{3}$$

The coordinates of points A (x_A and y_A), B (x_B and y_B), C (x_C and y_C), D (x_D and y_D) and F (x_F and y_F) can be easily obtained by combining the above (Eqs. 1–3), and the values are as follows respectively:

$$x_A = R_0\sin\theta_0,\ y_A = -R_0\cos\theta_0 + d \tag{4}$$

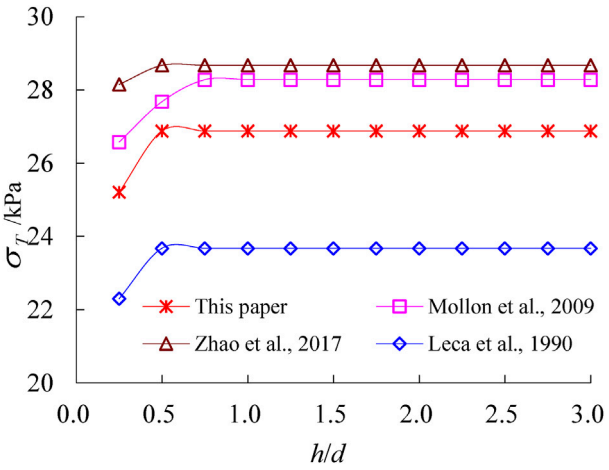

FIGURE 4
Calculated limit support pressure σ_T at given parameters (c = 7 kPa, φ=17°, γ =18 kN/m^3, D=10 m, σ_0 =0 kPa).

$$x_B = R_0\sin\theta_0,\ y_B = -R_0\cos\theta_0 + d \tag{5}$$

$$\begin{cases} x_C = R_0\sin\theta_0 + h/\left[\tan(\pi/4 + \varphi/2) - \tan\alpha\right] \\ y_C = \tan\alpha\cdot x_C + d + h - R_0\left[\cos\theta_0 + \tan\alpha\sin\theta_0\right] \end{cases} \tag{6}$$

$$\begin{cases} x_D = R_{OD}\cdot\sin\theta_d \\ y_D = -R_{OD}\cdot\cos\theta_d \\ R_{OD} = R_0\exp\left[(\theta_0 - \theta_d)\tan\varphi\right]\cdot\tan\alpha\cdot(R_0\sin\theta_0 - R_{OD}\sin\theta_c) \\ \qquad + R_0\cos\theta_0 - d - h - R_{OD}\cos\theta_d \end{cases} \tag{7}$$

$$\begin{cases} x_F = R_{OF}\cdot\sin\theta_f \\ y_F = -R_{OF}\cdot\cos\theta_f \\ R_{OF} = R_0\exp\left[\left(\theta_0 - \theta_f\right)\tan\varphi\right]\cdot\tan(\pi/4 + \varphi/2) \\ \qquad \cdot\left(R_0\sin\theta_0 - R_{OF}\sin\theta_f\right) \\ \qquad + R_0\cos\theta_0 - d - R_{OF}\cos\theta_f \end{cases} \tag{8}$$

From Eqs 4–8, the length R_{OD}, R_{OF}, L_{OB}, L_{OC}, L_{BC}, L_{CD} and L_{BF} can be obtained.

2.3 External load power

When the rigid slider $ABCD$ rotates around the center of rotation O (i.e., the origin of coordinates), the sliding surfaces AD and BC are velocity discontinuity surfaces. The power of the external work done by $ABCD$ due to its own weight can be obtained by adding the power algebraic of the external work done by the blocks OAB, OBC, OCD, and OAD. The specific expression of the power done by each block due to its own weight is as follows:

$$W_{OAB} = \frac{1}{3}\gamma(R_0\sin\theta_0)^2 d\omega \tag{9}$$

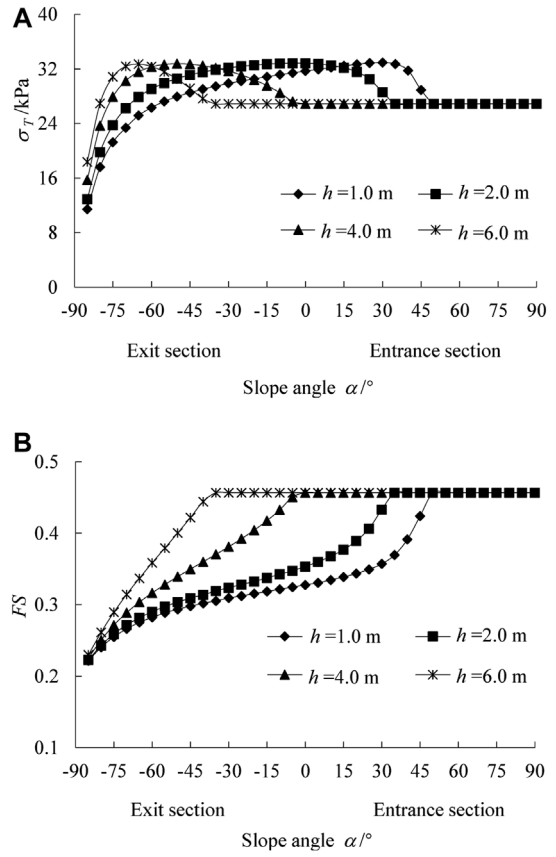

FIGURE 5
Limit support pressure σ_T and safety coefficient *FS* changing with slope angle α and burial depth *h* **(A)** σ_T; **(B)** *FS*.

$$W_{OBC} = \frac{1}{3}\gamma L_{OB} L_{BC} \sin\left(\theta_b + \frac{\pi}{4} - \frac{\varphi}{2}\right) \times \left[R_0 \sin\theta_0 + L_{BC} \cos\left(\frac{\pi}{4} + \frac{\varphi}{2}\right)\right]\omega \tag{10}$$

$$W_{OCD} = \frac{1}{3}\gamma L_{OC} R_{OD} \sin(\theta_d - \theta_c) \times [L_{OC} \sin\theta_c + L_{CD} \cos\alpha]\omega \tag{11}$$

$$W_{OAD} = \int_{\theta_0}^{\theta_d} \frac{\gamma R^2}{2} \cdot \frac{2}{3} R \sin\theta \cdot \omega \mathrm{d}\theta = \frac{R_0^3 \omega}{3(1+9\tan^2\varphi)} \cdot \begin{bmatrix} (\cos\theta_0 + 3\tan\varphi \sin\theta_0) \\ -(\cos\theta_d + 3\tan\varphi \sin\theta_d) \\ \times \exp[3(\theta_0 - \theta_d)\tan\varphi] \end{bmatrix} \tag{12}$$

As shown in Figure 3A, for the entrance section, the power of the external work done by *ABCD* due to its own weight is

$$W_G = W_{OAD} - W_{OAB} - W_{OBC} - W_{OCD} \tag{13}$$

and Eq. 13 is also applicable for the exit section when $(\pi/2+\alpha) > \theta c$ (as shown in Figure 3B, the corresponding α of the exit is a negative value). For the exit section when $(\pi/2+\alpha)<\theta c$, the power of external work done by *ABCD* due to its own weight is

$$W_G = W_{OAD} - W_{OAB} - W_{OBC} + W_{OCD} \tag{14}$$

When the intersection *F* between *AF* and *BF* is located inside the slope, the power of the external work done by the rigid slider *ABF* due to its own weight can be obtained by algebraically adding the external work power done by *OAB*, *OAF*, and *OBF*

$$W_{OAF} = \frac{R_0^3 \omega}{3(1+9\tan^2\varphi)} \begin{bmatrix} (\cos\theta_0 + 3\tan\varphi \sin\theta_0) \\ -(\cos\theta_f + 3\tan\varphi \cos\theta_f) \\ \times \exp[3(\theta_0 - \theta_f)\tan\varphi] \end{bmatrix} \tag{15}$$

$$W_{OBF} = \frac{1}{3}\gamma L_{OB} L_{BF} \sin\left(\theta_b + \frac{\pi}{4} - \frac{\varphi}{2}\right) \times \left[R_0 \sin\theta_0 + L_{BF} \cos\left(\frac{\pi}{4} + \frac{\varphi}{2}\right)\right]\omega \tag{16}$$

When the slider *ABF* is located inside the slope, the power of external work done due to its own weight is as follows:

$$W_G = W_{OAF} - W_{OAB} - W_{OBF} \tag{17}$$

The power W_0 and W_T of the external work done by the surface overload σ_0 and the supporting pressure σ_T on the tunnel excavation surface is as follows respectively:

$$W_0 = \frac{2}{3}\sigma_0 L_{CD} \cos\alpha [L_{OC} \cos\theta_d + L_{CD} \cos\alpha]\omega \tag{18}$$

$$W_T = \sigma_T d\left(R_0 \cos\theta_0 - \frac{d}{2}\right)\omega \tag{19}$$

2.4 Internal energy dissipation

According to the upper-bound theorem of limit analysis, the internal energy dissipation on the section between different speeds is calculated. The energy dissipation of the failure mode shown in Figure 3 includes the energy consumption on *AD* and *BC* on the top of the vault. The calculation formula is as follows:

$$D_{AD} = \int_{\theta_0}^{\theta_d} \frac{cR}{\cos\varphi} \cdot R\cos\varphi \cdot \omega \,\mathrm{d}\theta = \frac{cR_0^2\omega}{2\tan\varphi}\{1 - \exp[2(\theta_0 - \theta_d)\tan\varphi]\} \tag{20}$$

$$D_{BC} = cL_{BC} L_{OB} \sin\left(\theta_b + \frac{\pi}{4} - \frac{\alpha}{2}\right) \cos\varphi \cdot \omega \tag{21}$$

Then, the total internal energy dissipation on the sliding surface is

$$D = D_{AD} + D_{BC} \tag{22}$$

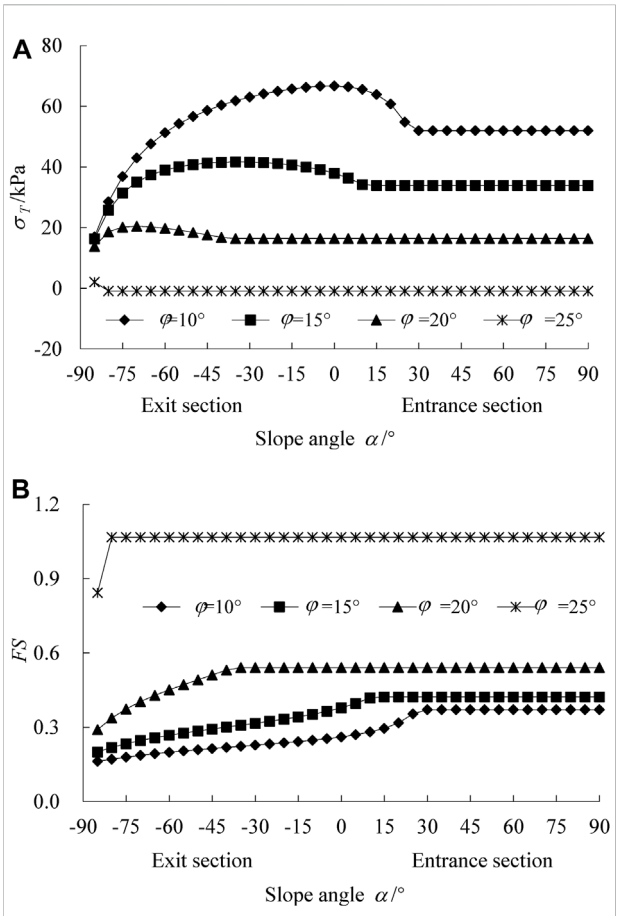

FIGURE 6
Limit support pressure σ_T and safety coefficient *FS* changing with slope angle α and internal friction angle φ: **(A)** σ_T; **(B)** *FS*.

When the intersection *F* between *AF* and *BF* is located inside the slope, the total internal energy dissipation on the sliding surface is

$$D = D_{BF} + D_{AF} = \frac{cR_0^2\omega}{2\tan\varphi}\left\{1 - \exp\left[2\left(\theta_0 - \theta_f\right)\tan\varphi\right]\right\} + cL_{OF}L_{OB}\sin\left(\theta_b + \frac{\pi}{4} - \frac{\alpha}{2}\right)\cos\varphi\cdot\omega \tag{23}$$

2.5 Calculation and verification

According to the virtual work principle in the limit analysis theory, the external load power is equal to the internal energy dissipation power, i.e. $D = W_G + W_0 + W_T$, and the objective function of the limit support pressure σ_T of the tunnel excavation face is obtained as follows:

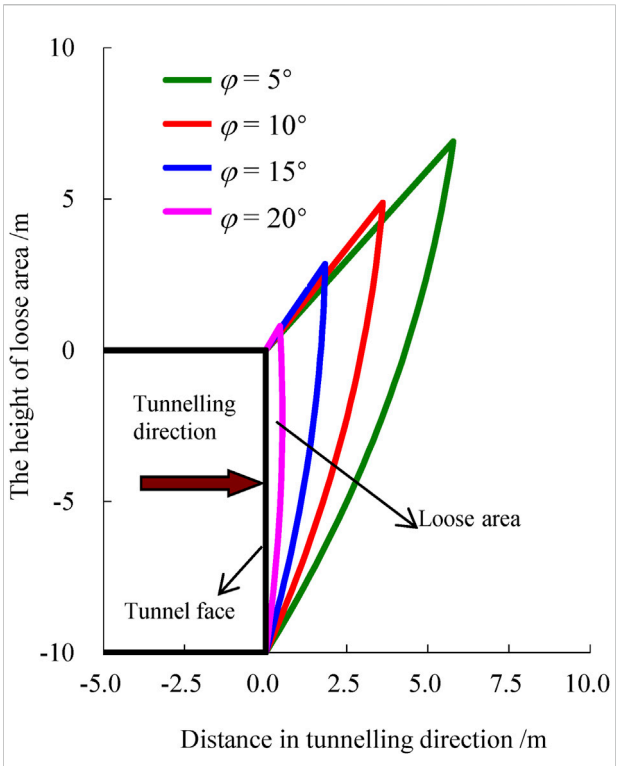

FIGURE 7
The effect of internal friction angle φ on the loose area.

$$\sigma_T = \frac{D - W_G - W_0}{d\left(R_0\cos\theta_0 - 0.5d\right)\cdot\omega} \tag{24}$$

The strength reduction method was adopted to obtain the safety coefficient *FS* of the tunnel face

$$FS = \frac{c}{c'} = \frac{\tan(\varphi)}{\tan(\varphi')} \tag{25}$$

where *c* and φ are the cohesion and friction angle of the surrounding rocks, respectively. And *c'* and φ' are the reduction parameters of the cohesion and friction angle for the failure of the excavation face, respectively. Substituting Eq. 25 into Eq. 24 so as to make sure σ_T of the tunnel face is equal to 0, and then *FS* of the tunnel face can be obtained.

Calculations of σ_T at given parameter values (*c* = 7 kPa, φ=17°, γ =18 kN/m^3, *D*=10 m, σ_0 =0 kPa) are carried out and comparisons with others are conducted. Graphically, the calculation results are depicted in Figure 4. It can be seen that the calculation results in this paper are very close to those in the existing literatures, which are 6.2 and 6.5% lower than those of Mollon et al. (2009) and Zhao et al. (2017), respectively, but are 11.9% higher than those of Leca and Dormieux. (1990). When *c*/*d* is greater than 0.6, the loose area is located inside the slope, and σ_T of the face is constant,

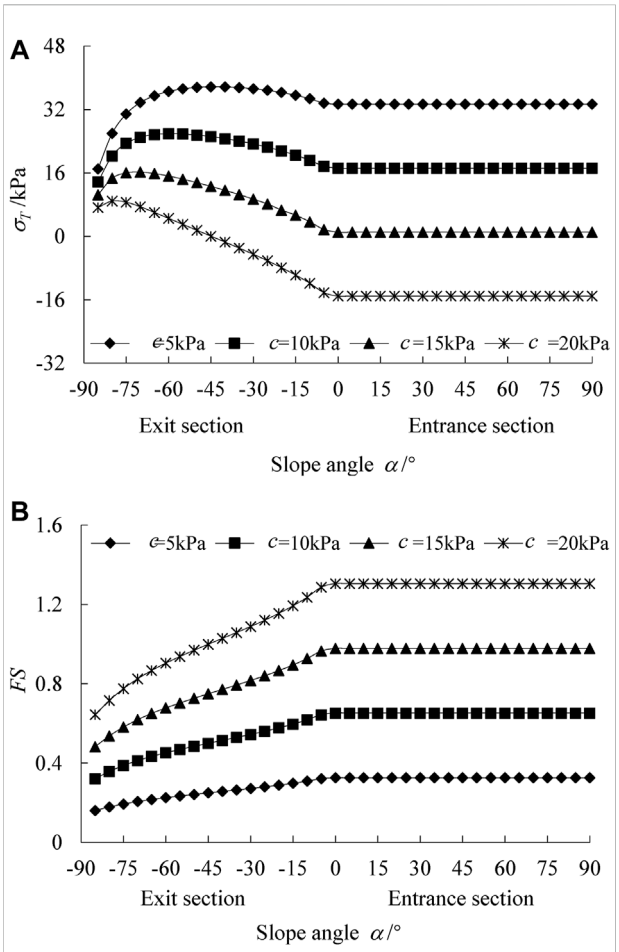

FIGURE 8
Limit support pressure σ_T and safety coefficient *FS* changing with slope angle and soli cohesion: **(A)** σ_T; **(B)** *FS*.

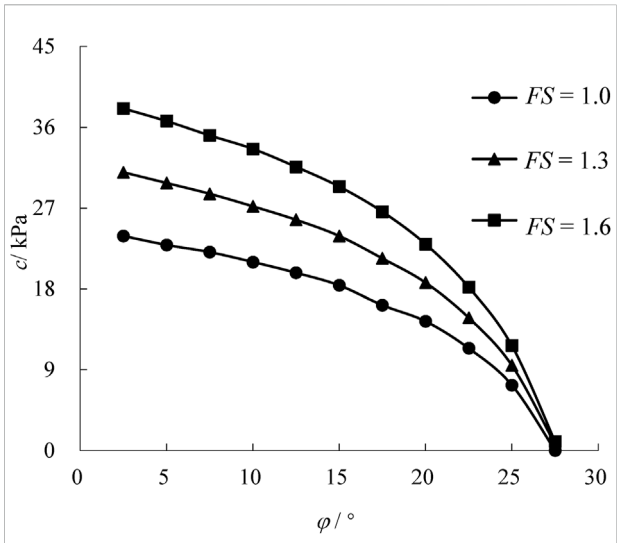

FIGURE 9
Change law of cohesion *c* and internal friction angle φ of the surrounding rock corresponding to different safety coefficients *FS* (α =10°, *d* =10 m, *h* = 10 m, and γ = 20 kN/m^3).

which is consistent with the actual situation. Through the above comparison and analysis, the rationality and correctness of the calculation method in this paper are verified.

3 Comparison in entering and exiting

The slope at the tunnel entrance and exit sections is indicated by α (a positive value representing the slope of the ground surface at the tunnel entrance section or a negative value representing the slope of the ground surface at the tunnel exit section). In order to analyze the influence of the surface slope at the tunnel entrance and exit sections on the stability of the tunnel surface, the following parameters are taken: D =10 m, h =4 m, γ =18 kN/m^3, c =7 kPa and φ=17°. When analyzing the influence of a certain factor on the stability of the tunnel face, other parameters shall remain unchanged.

3.1 Different burial depth

The relationships between the σ_T and *FS* of the tunnel face and the slope of the ground under the condition of different burial depth of the tunnel crown h are shown in Figure 5.

Figure 5A shows under the same h, with the increase of α, the σ_T of the face increases first, and then decreases to a certain value, and eventually goes steady. When the σ_T is constant, the loose area in front of the face will be all inside the slope, and the loose area no longer extends upward due to the arching effect of the surrounding rock, so the increase of h will not lead to the increase of σ_T. When the α is small, the loose area will shrink, thus the required σ_T will decrease; With the increase of α and the loose area, the increase of external load power will decrease gradually, while the increase of internal energy dissipation on the sliding surface is approximately a constant value (Figure 3), thus causing σ_T increasing first and then decreasing. In addition, it is easy to understand that the larger the h is, the smaller the corresponding α when reaching the maximum value and the constant value, and the change of h has no influence on the maximum value and the constant value of σ_T.

Figure 5B shows when h is the same, the *FS* of the face increases gradually with the increase of the surface slope until the loose area is completely inside the slope; when the α remains a small value, the larger the h is, the larger the corresponding *FS* is. When α = −70° and H = 1.0 m, the corresponding *FS* and σ_T are the smallest; when α = −15° and H = 1.0 m, the corresponding *FS* is the largest, but the σ_T is the largest.

According to the above results, the stability of the tunnel face at the exit section is lower than that at the entrance section. When

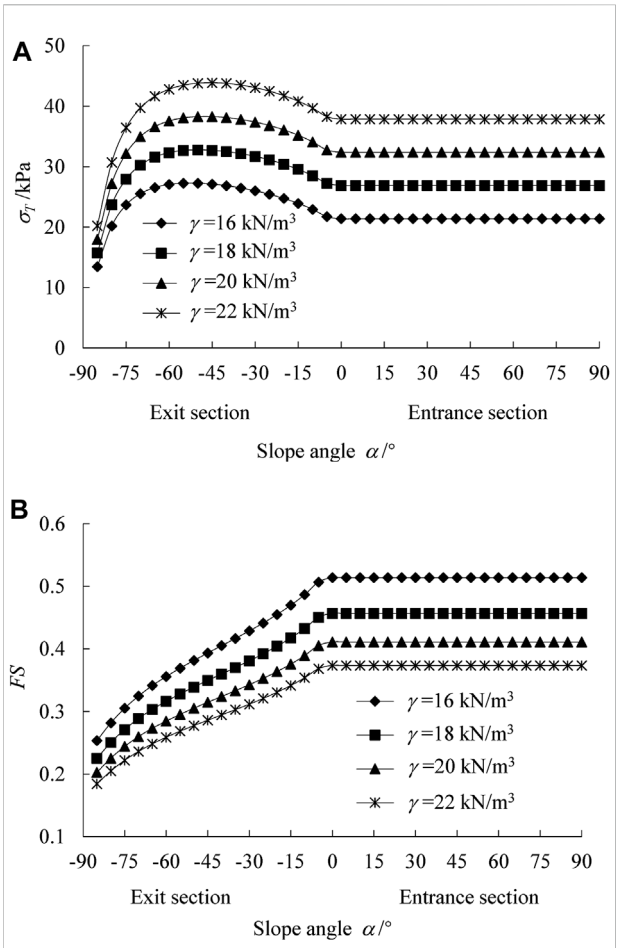

FIGURE 10
Limit support pressure σ_T and safety coefficient *FS* changing with slope angle and unit weight of surrounding rock: **(A)** σ_T; **(B)** *FS*.

the loose area is completely located inside slope, the stability of the excavation face are the highest.

3.2 Strength parameters of different surrounding rocks

3.2.1 Internal friction angle φ

When the internal friction angle φ of the surrounding rock is different, the relationship between the σ_T and *FS* of the tunnel face and the surface slope α is shown in Figure 6.

It can be seen that when h is constant and φ is small, the σ_T of the face increases with the increase of α and then decreases, and finally tends to be constant; *FS* of the face gradually increases with the increase of α, and finally reaches a constant value; the larger the φ is, the smaller the α is when σ_T and *FS* reach constant values. When the α is large, σ_T and *FS* of the face are both constant; when α is constant, the larger the φ is, the smaller the corresponding σ_T is, and the larger the *FS* is. The main reason is that the increase of φ makes the loose area in front of the face decrease significantly, resulting in a significant reduction of external load power, as shown in Figure 7. And when the σ_T and *FS* are constant, it means that the loose area of the surrounding rock is completely located inside the slope, and the loose area is no longer developed upward due to the arching effect of the surrounding rock.

3.2.2 Cohesion c

Under different cohesion c, the relationship between the σ_T and *FS* of the tunnel face and the surface slope α is shown in Figure 8. When α is constant, the σ_T decrease linearly with the increase of c, while *FS* increase linearly with the increase of c.

When the surface is horizontal (i.e., $\alpha = 0^{\circ}$), the change law of c and φ corresponding to different *FS* are shown in Figure 9. The values of other parameters are as follows: d =10 m, h = 10 m, and γ = 20 kN/m³. It can be seen that c and φ can significantly affect the *FS*. When the *FS* of the face is constant, the required c decreases gradually with the increase of the φ, and the decreasing amplitude increases gradually. The larger the φ is, the smaller the difference in c required to meet the requirements of different stability factors of the excavation face is.

3.3 Unit weight of the surrounding rock γ

Under the condition of different unit weight γ of surrounding rocks, the relationship between σ_T and *FS* of the tunnel face and α is shown in Figure 10. It can be seen that when the α is the same, the σ_T and *FS* of the tunnel face decrease and increase linearly with the increase of γ, respectively.

4 Conclusions and perspectives

Based on the upper-bound theorem of limit analysis, a calculation method to quantitatively analyze the limit support pressure σ_T and safety coefficient *FS* of the tunnel face is put forward. Compared with the existing literature results, the correctness and effectiveness of this method adopted in this paper are verified. By using such method, the calculation of the σ_T and *FS* of the tunnel face under the conditions of different surface slopes α at the tunnel entrance and exit sections is carried out. The following conclusions are drawn:

1) The σ_T of the tunnel face increases first and then decreases with the increase of α and finally reaches a constant value; the *FS* increases gradually with the increase of α, and goes steady when α increases to a certain value.
2) When α is small, the *FS* of the tunnel face gradually increases with the increase of the burial depth of the tunnel crown h; when the loose area in front of the excavation is completely

located inside the slope, the loose area no longer develops upward due to the arching effect, so when the slope increases by a certain amount, the σ_T and *FS* of the tunnel face are no longer affected by the change of *h*.

3) The cohesion *c* and internal friction angle φ of the surrounding rock can significantly affect the σ_T and *FS* of the face. The increase of φ will obviously reduce the loose area in front of the face and will significantly improve the face stability; when the α is constant, the σ_T and *FS* of the face increase linearly with the increase of *c* and unit weight of the surrounding rock γ. The larger the φ is, the smaller the difference in *c* required to meet the requirements of different safety coefficients of the excavation face is.
4) For shallow buried tunnel, the *FS* of exiting is relatively low compared with that of entering. Therefore, more attention should be paid during the excavation of exiting the tunnel.
5) Research results show that the face stability between entering and exiting excavation is different for the shallow-buried tunnel with a front slope, which can serve as references for the excavation and support of this portal. Further research can be carried out for other types of tunnel portals, such as the shallowly buried and asymmetrically loaded tunnel portal.

Data availability statement

The raw data supporting the conclusions of this article will be made available by the authors, without undue reservation.

Author contributions

XZL: resources, data curation, project; investigation. XLL Calculation: Theoretical methods; validation. CY: writing-original draft preparation; editing; project.

Funding

This work is supported by the National Natural Science Foundation of China (No. 42177132); Natural Science Foundation of Hubei Province (Nos. 2021CFA090 and 2021CFB536); the Open Fund of Key Laboratory of Geological Hazards on Three Gorges Reservoir Area (China Three Gorges University), Ministry of Education (2015KDZ04).

Conflict of interest

The authors declare that the research was conducted in the absence of any commercial or financial relationships that could be construed as a potential conflict of interest.

Publisher's note

References

Adam, D., Markiewicz, R., and Brunner, M. (2014). Block-in-matrix structure and creeping slope: Tunneling in hard soil and/or weak rock. *Geotech. Geol. Eng. (Dordr).* 32 (6), 1467–1476. doi:10.1007/s10706-012-9591-5

Anagnostou, G., and Perazzelli, P. (2013). The stability of a tunnel face with a free span and a non-uniform support. *Geotechnik* 36 (1), 40–50. doi:10.1002/gete.201200014

Broms, B. B., and Bennermark, H. (1967). Stability of clay at vertical opening. *J. Soil Mech. Found. Div.* 93 (1), 71–94. doi:10.1061/jsfeaq.0000946

Chambon, P., and Corté, J. F. (1994). Shallow tunnels in cohesionless soil: Stability of tunnel face. *J. Geotech. Engrg.* 120 (7), 1148–1165. doi:10.1061/(asce)0733-9410(1994)120:7(1148)

Coulter, S., and Martin, C. D. (2006). Effect of jet-grouting on surface settlements above the Aeschertunnel, Switzerland. *Tunn. Undergr. Space Technol.* 21 (5), 542–553. doi:10.1016/j.tust.2005.07.005

Cui, S., Pei, X., Jiang, Y., Wang, G., Fan, X., Yang, Q., et al. (2021). Liquefaction within a bedding fault: Understanding the initiation and movement of the Daguangbao landslide triggered by the 2008 Wenchuan Earthquake (Ms = 8.0). *Eng. Geol.* 295, 106455. doi:10.1016/j.enggeo.2021.106455

He, Y., and Kusiak, A. (2017). Performance assessment of wind turbines: Data-derived quantitative metrics. *IEEE Trans. Sustain. Energy* 9 (1), 65–73. doi:10.1109/tste.2017.2715061

Kontogianni, V., Tzortzis, A., and Stiros, S. (2004). Deformation and failure of the tymfristos tunnel, Greece. *J. Geotech. Geoenviron. Eng.* 130, 1004–1013. doi:10.1061/(asce)1090-0241(2004)130:10(1004)

Leca, E., and Dormieux, L. (1990). Upper and lower bound solutions for the face stability of shallow circular tunnels in frictional material. *Geotechnique* 40 (4), 581–606. doi:10.1680/geot.1990.40.4.581

Lei, M. F., Peng, L. M., and Shi, C. H. (2015). Model test to investigate the failure mechanisms and lining stress characteristics of shallow buried tunnels under unsymmetrical loading. *Tunn. Undergr. Space Technol.* 46, 64–75. doi:10.1016/j.tust.2014.11.003

Li, H., Deng, J., Feng, P., Pu, C., Arachchige, D., and Cheng, Q. (2021a). Short-term nacelle orientation forecasting using bilinear transformation and ICEEMDAN framework. *Front. Energy Res.* 9, 780928. doi:10.3389/fenrg.2021.780928

Li, H., Deng, J., Yuan, S., Feng, P., and Arachchige, D. (2021b). Monitoring and identifying wind turbine generator bearing faults using deep belief network and EWMA control charts. *Front. Energy Res.* 9, 799039. doi:10.3389/fenrg.2021.799039

Li, H., He, Y., Xu, Q., Deng, j., Li, W., and Wei, Y. (2022). Detection and segmentation of loess landslides via satellite images: A two-phase framework. *Landslides* 19, 673–686. doi:10.1007/s10346-021-01789-0

Li, J. M., and Yang, C. (2016). Impact of excavation sequence from inside on surrounding rock stability at the portal of a shallow and unsymmetrically loaded tunnel. *Electron. J. Geotechnical Eng.* 21 (13), 4739–4749.

Li, T. J. (2009). Cause analysis of tunnel initial support deformation and the treatment. *Highw. Auto Appl.* 4 (3), 197–199. (in Chinese). doi:10.3969/j.issn.1671-2668.2009.03.063

Liang, Q., Yang, X. L., and Chen, X. (2017). Limit equilibrium analysis of round length in tunnel excavation. *J. South China Univ. Technol. Nat. Sci. Ed.* 45 (5), 123–119. (in Chinese). doi:10.3969/j.issn.1000-565X.2017.05.016

Liu, X. J., Yang, C., and Yu, J. (2015). The influence of moisture content on the time-dependent characteristics of rock material and its application to the construction of a tunnel portal. *Adv. Mater. Sci. Eng.* 2015, 1–13. doi:10.1155/2015/725162

Miura, K. (2003). Design and construction of mountain tunnels in Japan. *Tunn. Undergr. Space Technol.* 18, 115–126. doi:10.1016/s0886-7798(03)00038-5

Mollon, G., Dias, D., and Soubra, A. H. (2009). Probabilistic analysis and design of circular tunnels against face stability. *Int. J. Geomech.* 9 (6), 237–249. doi:10.1061/(asce)1532-3641(2009)9:6(237)

Takano, D., Otani, J., Fukushige, S., and Natagani, H. (2010). Investigation of interaction behavior between soil and face bolts using X-ray CT. *Adv. X-ray Tomogr. Geomaterials* 26 (4), 389–395. doi:10.1002/9780470612187.ch41

Wu, J., Liao, S. M., and Shi, Z. H. (2015). Workface stability of shield tunnel considering arching effect. *J. Tongji Univ. Nat. Sci.* 43 (2), 213–220. (in Chinese). doi:10.11908/j.issn.0253-374x.2015.02.008

Xiao, J. Z., Dai, F. C., Wei, Y. Q., Xing, Y. C., Cai, H., and Xu, C. (2016). Analysis of mechanical behavior in a pipe roof during excavation of a shallow bias tunnel in loose deposits. *Environ. Earth Sci.* 75 (4), 293. doi:10.1007/s12665-015-5176-y

Yang, C., Chen, Y. H., Guo, Z., and Wang, R. H. (2021). Surface settlement control in the excavation of a shallow intersection between a double-arched tunnel and a connection. *Tunn. Int. J. Geomechanics* 24 (4), 04021035. doi:10.1061/(ASCE)GM.1943-5622.0001983

Yang, C., Chen, Y. H., Huang, D., and Wang, L. H. (2019). Arching effect between the pipes of a pipe umbrella support system in a shallow-buried tunnel. *KSCE J. Civ. Eng.* 23 (12), 5215–5225. doi:10.1007/s12205-019-5197-2

Yang, C., Hu, Z. X., Huang, D., and Guo, F. (2019). Failure mechanism of primary support for a shallow and asymmetrically loaded tunnel portal and treatment measures. *J. Perform. Constr. Facil.* 34, 0001385. doi:10.1061/(ASCE)CF.1943-5509.0001385

Ye, F., He, C., Wang, S. M., and Zhang, J. L. (2012). Landscape design of mountain highway tunnel portals in China. *Tunn. Undergr. Space Technol.* 29, 52–68. doi:10.1016/j.tust.2012.01.001

Yuan, B. X., Sun, M., Xiong, L., Luo, Q. Z., Pradhan, S. P., and Li, H. Z. (2020). Investigation of 3D deformation of transparent soil around a laterally loaded pile based on a hydraulic gradient model test. *J. Build. Eng.* 28 (3), 101024. doi:10.1016/j.jobe.2019.101024

Zhang, C., Han, K., and Zhang, D. (2015). Face stability analysis of shallow circular tunnels in cohesive–frictional soils. *Tunn. Undergr. Space Technol.* 50, 345–357. doi:10.1016/j.tust.2015.08.007

Zhao, L., Li, D., Li, L., Feng, Y., Cheng, X., and Luo, W. (2017). Three-dimensional stability analysis of a longitudinally inclined shallow tunnel face. *Comput. Geotechnics* 87, 32–48. doi:10.1016/j.compgeo.2017.01.015

Zhou, J., Wei, J., Yang, T., Zhang, P., Liu, F., and Chen, J. (2021). Seepage channel development in the crown pillar: Insights from induced microseismicity. *Int. J. Rock Mech. Min. Sci.* 145, 104851. doi:10.1016/j.ijrmms.2021.104851